CRYSTAL GROWTH & DESIGN

pubs.acs.org/crystal

Article

Seeding Layer Approach for the Synthesis of Co-ZIF-90 Thin Films of Optical Quality

Nils Christian Keppler, Johanna Fricke, Andreas Schaate, Adrian Hannebauer, Karen Deli Josephine Hindricks, Saskia Zailskas, and Peter Behrens*

Cite This: *Cryst. Growth Des.* 2022, 22, 7008−7020

Read Online

ACCESS | Metrics & More | Article Recommendations | Supporting Information

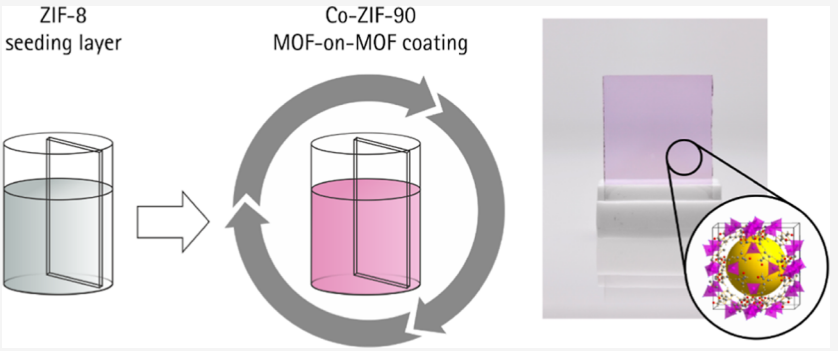

ABSTRACT: The growth of zeolitic imidazolate framework (ZIF) thin films is an interesting topic, since ZIFs have a high thermal and chemical stability compared to many other MOFs. A variety of functionalities can be introduced via the imidazole linker molecule. Here, we report on a new approach for the preparation of thin films of a novel ZIF material: Co-ZIF-90. The preparation of thin films is possible on silicon or glass when ZIF-8 seeding layers are deposited first. The resulting constructions are effectively MOF-on-MOF layer systems. The synthesis procedure has been optimized with regard to obtaining high-quality thin films of Co-ZIF-90 on ZIF-8 for optical applications. Notably, the preparation of Co-ZIF-90 thin films is possible only by using a mixture of two different cobalt precursor salts (acetate and nitrate). The thin films are characterized in detail. With regard to the use as an optical material, UV−vis absorption spectra of the MOF-on-MOF constructs were measured and the refractive index of Co-ZIF-90 was determined using ellipsometry. Furthermore, the refractive index of the Co-ZIF-90 film can be modulated reversibly by the adsorption and desorption of water via the gas phase. The kinetics of this fast process are on the time scale of 1 s. In addition to the preparation of thin films, we obtained Co-ZIF-90 as a powder sample and basically characterized the powder. The approach to use an easy-to-crystallize ZIF-8 film as a seeding layer for the growth of films of other ZIFs may be extended as a general concept for the deposition of crystalline ZIF layers in such cases, where a direct deposition is difficult or not possible.

1. INTRODUCTION

Metal−organic frameworks (MOFs) are highly porous hybrid materials built of inorganic building units (IBUs) and organic linker molecules.[1] The linker molecules have at least two functional groups, which are used to connect the IBUs. Most MOFs possess linkers with carboxylate as coordinating functional group,[1−3] but other functional groups like amines can also be used for the coordination of the IBUs.[4,5] As a porous material, MOFs have high inner surface areas of up to a few thousand m^2/g,[6] enabling a variety of applications, like gas storage[7−9] and gas separation,[10−12] sensing,[13,14] and catalysis.[15,16] Furthermore, MOFs gain increasing interest in nonclassical application fields like biomedical technology[17−19] as well as electronics, optics and optoelectronics.[20−23] Still hampering the further translation into real-world applications is the fact that for many practical applications, the MOF has to be shaped into a specific morphology, like monoliths (pellets, tablets, and granules), gels or foams, membranes, or thin films as well as composite materials (e.g., on fibers or nanosheets).[24,25] For the deposition of MOF membranes and thin films, different supports like fibers,[26−28] porous disks,[29,30] nanosheets,[31,32] and flat surfaces (e.g., glass, silicon, and gold surfaces)[33−35] can be used.

Zeolitic imidazolate frameworks (ZIFs) are an interesting subgroup of MOFs. In ZIFs, imidazolate or a derivative thereof serves as a linker. The IBUs are connected by the nitrogen atoms of the imidazolate rings. Due to a tetrahedral

Received: June 14, 2022
Revised: November 1, 2022
Published: November 28, 2022

coordination of the metal ions in ZIFs and similar bond angles of Si−O−Si linkages in zeolites and N−[M]−N linkages in ZIFs, the structures of ZIFs possess strong structural similarities with zeolites. In most cases, Zn^{2+} ions function as metal ions in ZIFs; however, ZIFs containing other metal ions like Co^{2+}, Cu^{2+}, and Cd^{2+} are also known.[4,36] Of these, those with transition metal ions with a d electronic sub-shell not fully occupied may feature additional functionalities.

MOF thin films can be prepared by different fabrication techniques, ranging from liquid-phase epitaxy (LPE), carried out using dip-coating, spray-coating, spin-coating, or flowing techniques,[33,37−39] to direct growth[35,40] and secondary growth methods.[26,30] UiO-66, Cu-BDC, and especially HKUST-1 MOFs are widely used as model systems.[33,41] In nearly all cases, a thin film of only one single MOF is coated onto a substrate. Only a few reports have elucidated the possibility to prepare a MOF film on top of another MOF film (MOF-on-MOF coatings). In most of these publications, LPE techniques were used.[42−47] Knebel et al. used an LPE-based flow technique to grow ZIF-8 on ZIF-67.[42] Both ZIFs have the same linker (2-methylimidazolate) and differ only in the metal ion (ZIF-8: Zn^{2+}, ZIF-67: Co^{2+}). Thus, both MOFs are isostructural and possess nearly the same unit cell parameters. In a similar vein, Shekhah et al.[43] grew $[Zn_2(NDC)_2DABCO]$ on the copper version of the MOF with the same linkers, also using LPE, employing dip-coating. Again, the unit cell parameters are practically equal. In both reports, the synthesis procedures took around 1 week, which is in general a large drawback of most LPE methods, except for when spray-coating is used.[33] This method was applied by the groups Yao et al.[44] and Wang et al.[45] Both groups first functionalized gold surfaces with self-assembled monolayers (SAMs) to obtain activated surfaces for MOF growth. Yao et al.[44] combined spray-coating, which was used to grow a bottom layer of Cu-HHTP, with a stamp-based method, which was employed to deposit pre-synthesized layers of nanosheets of Cu- or Zn-TCPP. Wang et al.[45] used the LPE spray-coating technique for the generation of three different MOF layers (Cu-BDC, Cu-NDC, and Cu-BPDC). These MOFs have the same topology but show a large mismatch in their cell parameters. Nevertheless, it was possible to obtain MOF-on-MOF or MOF-on-MOF-on-MOF systems of these frameworks, respectively. Oldenburg et al.[46] also used the LPE spray-coating approach for the growth of an A−B−A stack of Zn(ADB) and Zn(Pd-DCP). A different method was used by Ikigaki et al.: these authors used substrates covered with thin $Cu(OH)_2$ films that were in the first step (partly) converted to a MOF by incubating them into saturated solutions of the BPDC or the BDC linker. In the next step(s), one (or two) more Cu-MOF thin films were coated on the first thin film using LPE dip-coating.[47] This short overview illustrates that only a few methods have so far been employed to produce MOF-on-MOF layer systems. Most of these techniques are time-consuming, either because of necessary pretreatments of the substrate (e.g., formation of a SAM), the synthesis itself (most LPE methods, e.g., dip-coating or flowing techniques), or due to the fact that they require a combination of different methods to enable the formation of a stack of MOF films. Also, methods like stamping, while being fast and versatile, may lead to inclusions or empty pores at the interface and thus to defective staples.

Thin films of ZIF-7, ZIF-9, ZIF-65-Zn, ZIF-67, and ZIF-90 have already successfully been grown on silica surfaces (SiO_2-coated QCMs or silicon wafers),[48] but only thin films of ZIF-8 have so far been presented in optical quality, that is, with high homogeneity, absence of scattering, and high transparency.[35,49] It has been shown that ZIF-8 can be used for optical switching on different substrates like glass or silicon[35,49] but also on coated optical fibers.[27,50] Optical quality becomes important when the thin films are to be used in real-world technical devices, where signal losses due to, for example, scattering are critical. Usually, optical quality cannot be achieved when the films are deposited from a nanoparticle suspension. Albeit simple to execute, such methods typically lead to inhomogeneities and voids in the thin films.[41,51] Dense thin films which are fabricated directly from the precursor solution show a much higher quality.[35,48,49]

In the present work, we have therefore concentrated on the promising cycle-based direct growth procedure, which had been reported for the growth of ZIF-8 thin films of optical quality before.[35,49] Here, we extend this work to prepare MOF-on-MOF systems where the high-quality ZIF-8 coating is used as a seeding layer for the growth of thin films of Co-ZIF-90. ZIF-8 and ZIF-90 both crystallize in the **sod** topology, as do a variety of other ZIFs.[36] ZIF-90 is known in its zinc variant;[52] Co-ZIF-90, built exclusively with cobalt as the coordinated metal, has—to the best of our knowledge—not been reported before. The only report in this field is about amorphous ZIF-90 particles that were post-synthetically doped with cobalt for the production of a carbon material.[53] Here, we have obtained Co-ZIF-90 as thin film and in powder form. ZIF-90 MOFs are of special interest because they contain the imidazolate 2-carbaldehyde linker; the aldehyde group could be employed in post-synthetic modification reactions.[52]

2. MATERIALS AND METHODS

2.1. Materials. Zinc(II) nitrate hexahydrate (98%, Sigma-Aldrich), 2-methylimidazole (99%, Sigma-Aldrich), cobalt(II) acetate tetrahydrate (98%, Sigma-Aldrich), cobalt(II) nitrate hexahydrate (98%, Roth), imidazole-2-carboxaldehyde (97%, Fisher Scientific), methanol (99.5%, Roth), ethanol (99.8%, Fisher Scientific, dry), dimethylformamide (99.8%, Sigma-Aldrich, DMF), sulfuric acid (96%, Roth), and hydrogen peroxide (35%, Roth) were used without further purification.

Sb-doped silicon wafers with 111-orientation were applied as substrates for all syntheses "on silicon." The wafers were cut into pieces of 1 × 1 cm (for most of the characterizations methods) or 2 × 2 cm (for krypton physisorption). For the thin film growth "on glass," glass slides were cut into pieces of 22 × 25 mm (for UV/vis measurements) or 15 × 15 mm (for photographies). All substrates were cleaned in a fresh mixture of sulfuric acid and hydrogen peroxide (2:1) for 15 min. Subsequently, they were washed with water and methanol. Cleaned substrates were not stored but used directly.

2.2. Synthesis of ZIF-8 and Co-ZIF-90-on-ZIF-8 Thin Films. All reactions were performed at room temperature (18 °C).

We prepared the following stock solutions: 25 mM zinc(II) nitrate hexahydrate in methanol ("Zn"), 50 mM 2-methylimidazole in methanol ("HmIm"), imidazole-2-carbaldehyde in DMF with different concentrations ranging from 40 to 75 mM ("HImCA"), and Co^{2+} solutions in methanol with different concentrations ranging between 10 and 18.75 mM ("Co"). We used two different cobalt(II) precursor salts: cobalt(II) nitrate hexahydrate and cobalt(II) acetate tetrahydrate. We also used cobalt(II) solutions containing both precursors, with nitrate to acetate ratios of 0, 25, 33, 50, and 100%. After initial exploration, the ratio between the two cobalt(II) salts was set to two parts of the nitrate and one part of the acetate salt (33% acetate) for most syntheses. The solution of imidazole-2-carbaldehyde was prepared by stirring the linker in DMF at 70 °C for up to 60 min, depending on the concentration. All other solutions were prepared by stirring the linker or metal salt in methanol at room temperature until

https://doi.org/10.1021/acs.cgd.2c00664
Cryst. Growth Des. 2022, 22, 7008−7020

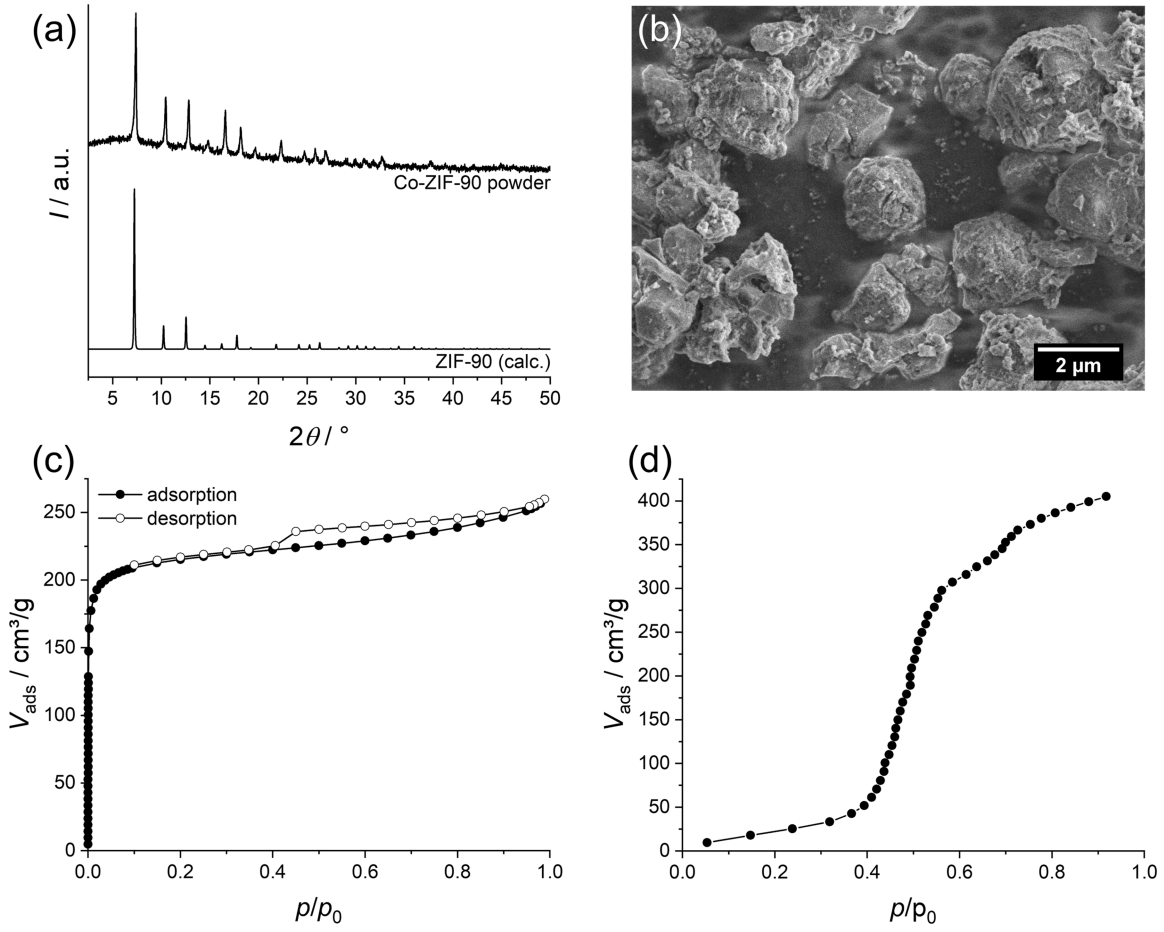

Figure 1. XRD pattern (a), SEM image (b), argon physisorption isotherm (c), and static water sorption isotherm (d) of Co-ZIF-90 particles. A calculated XRD pattern of ZIF-90 is given as a reference in (a).[52]

dissolved. The solutions are designated by "Zn,", "HmIm," "HImCA," and "Co" in the following.

The fabrication of Co-ZIF-90-on-ZIF-8 coatings is a two-step process: the first step is the growth of a ZIF-8 seeding layer, and the second step is the growth of Co-ZIF-90 on top of the ZIF-8 seeding layer. According to Lu and Hupp,[35] the ZIF-8 growth is started by mixing equal volume of "Zn" and "HmIm" in a glass vessel. A substrate is directly immersed in this synthesis solution after mixing the precursor solutions. After 30 min, the substrate is removed from the ZIF-8 synthesis solution and washed with methanol. The second step is started by directly immersing the freshly washed substrate from step one in a freshly prepared mixture of equal volume of "Co" and "HImCA." After 30 min, the substrate is removed from the synthesis solution and washed with methanol. Thicker Co-ZIF-90 thin films can be deposited by repeating step two as often as desired. It is important that the substrate is directly reincubated after rinsing; intermittent drying between steps one and two will lead to crack formation, as we have also experienced in the synthesis of high-quality ZIF-8 films.[49] After the final deposition cycle, the coated substrate is washed with methanol and incubated in dry ethanol over night to extract unreacted precursors from the pores.

The synthesis conditions for the growth of Co-ZIF-90 were optimized by exploring the precursor concentrations and by variation of the ratio of cobalt(II) acetate to cobalt(II) nitrate in the cobalt solution ("Co"). In all syntheses, the molar ratio of HImCA to Co^{2+} was kept at 4:1. Additionally, the reaction time in step two (Co-ZIF-90 growth) was adjusted between 30 and 60 min per deposition cycle.

2.3. Synthesis of Co-ZIF-90 Powder Samples. Co-ZIF-90 particles were synthesized by mixing solutions of imidazole-2-carbaldehyde (100 mM in DMF) and cobalt(II) acetate tetrahydrate (25 mM in methanol). The joint solution becomes turbid directly after mixing at room temperature. The mixture was stirred for 120 min and centrifuged afterward for 10 min at 6000 rpm. The solid was washed two times with fresh methanol, each washing procedure being followed by centrifugation for 10 min at 6000 rpm. Drying of the particles was performed at reduced pressure. The dry particles were used for X-ray diffraction (XRD), scanning electron microscopy (SEM), and sorption experiments.

2.4. Characterization of Thin Films and Powders. XRD measurements on ZIF-8 thin films were carried out with an X-ray diffractometer from STOE working in Bragg−Brentano geometry. An ISO-Debyeflex 3003 was used for the generation of X-rays at 40 kV and 30 mA, delivering Cu $K\alpha_1$ radiation. Measurements were carried out between 5° and 30° 2θ with a step size of 0.02° 2θ and a measurement time of 8 s per step.

A Sentech SE800 spectroscopic ellipsometer with a spectral range from 400 to 850 nm was used for the ellipsometry measurements. All measurements were performed at 70°. Ellipsometry data were fitted with a Cauchy dispersion model (ZIF-8) and a Tauc−Lorentz model (Co-ZIF-90). More information on the models used in the evaluation of ellipsometry data is given in the Supporting Information (see Table S1 and the explanatory text). Ellipsometry measurements were also carried out at different relative humidity (RH) using the humidity controller RH-200 (Porotec). The RH was checked directly before the inlet of the measurement cell with an external humidity sensor (Rotronic). Relative humidity values were calibrated using salt solutions with known RH. Argon was used as the feed gas.

Coated glass slide samples for SEM were prepared by fixing the specimen samples on SEM metal substrate holders with carbon tape. Electrical contact of the thin films was ensured by the use of a silver conductive lacquer and by sputtering the samples with a thin layer of gold. Most SEM images were recorded with a JSM-6610L V (Joel).

https://doi.org/10.1021/acs.cgd.2c00664
Cryst. Growth Des. 2022, 22, 7008−7020

Images were taken at 10 kV with a working distance of 10 mm. Cross-sectional images and images of the Co-ZIF-90 particles were recorded using a Regulus SU8200 (Hitachi). Images were typically recorded at a voltage of 2 kV and a current of 10 μA.

UV/vis spectra on glass substrates were recorded in transmission with a Cary 4000 (Agilent Technologies) in a maximum spectral range from 300 to 800 nm using the software "Scan." UV/vis kinetic experiments were performed with the software "Kinetics" belonging to the software package of the UV/vis spectrometer. For kinetic measurements, the transmission of the samples at 350 nm was measured every 0.1 s. We used a home-built UV/vis measurement cell with quartz glass windows that can be mounted tightly into the spectrometer. The atmosphere was changed in different time steps using dry argon and moist argon (obtained by bubbling argon through a water reservoir). A detailed explanation of the experiment and the results of a reference experiment on a ZIF-8-coated glass slide are given in the Supporting Information.

Atomic force microscopy (AFM) measurements were performed using an NX 10 by Park System Corp. All images were taken in noncontact mode with a scan rate of 0.5 Hz. The software "XEI" (5.2.0 by Park System Corp.) was used for the data analysis.

The XPS depth profiling was performed with a PHI VersaProbe III (Physical Electronics GmbH) XPS system. The chemical state of the material was analyzed using microfocused Al Kα X-rays (1486.7 eV, 50 W, 15 kV) with an X-ray spot size of 200 μm in diameter; dual-beam charge neutralization (a 1 V electron beam and a 7 V Ar^+ ion beam) was applied during measurements. For the sputter phase (6 s for every sputtering step), a 20 kV argon gas cluster ion beam with a sputter raster size of 2 mm × 2 mm was used. The acquired data were processed and evaluated using the MultiPak Software (ULVAC-PHI).

Krypton physisorption isotherms were recorded using an Autosorb 1 instrument from Quantachrome. The isotherms were evaluated with the software ASiQwin 2.0 from Quantachrome. Samples were outgassed at 120 °C for 24 h at reduced pressure. Measurements were performed at 87.15 K (liquid argon). The Brunauer–Emmett–Teller (BET) equation was applied to determine the BET surface areas.

The argon physisorption isotherm of the Co-ZIF-90 powder was measured at 87 K with a 3Flex instrument from micromeritics. 40 mg of the powder was activated at 120 °C for 24 h under vacuum prior to the measurement. The associated software from micromeritics was used for the analysis of the data (Version 5.02). BET surface areas were determined by the BET-auto function of the software.

Static water sorption isotherms of Co-ZIF-90 powders were recorded on a vapor 1000C from 3P instruments. A powder sample (50 mg) was activated at 120 °C for 20 h under vacuum. In situ activation at 120 °C for 4 h was performed additionally before the measurement. The isotherms were recorded at 25 °C.

3. RESULTS AND DISCUSSION

Thin films of different ZIFs can be grown directly at room temperature.[48] In these procedures, it is very important to control the synthesis parameters because the type of metal precursor, small changes of the precursor concentrations, and pretreatment of the substrate, like seeding, can all largely influence the MOF thin film growth.[26,48] It is worth noting that for Co-ZIF-90 thin films, we have found only a strictly limited synthesis window, as detailed below. In the course of this work, powders of Co-ZIF-90 were also obtained.

3.1. Co-ZIF-90 in Powder Form. During our studies on the formation of Co-ZIF-90 films on ZIF-8 seeding layers (see Section 3.3), we performed syntheses using cobalt(II) acetate as the cobalt source. Upon mixing solutions of imidazole-2-carboxaldehyde ("HImCA") in DMF and cobalt(II) acetate in methanol, precipitation occurs immediately. The resulting precipitate can be isolated as a purple, crystalline powder. The positions of the XRD reflections show good agreement with the calculated reflections of ZIF-90 (see Figure 1a).[52] Particles with a spherical shape and a diameter of ca. 2 μm which are built up from nanocrystals and feature a rough surface can be observed in the SEM images (see Figures 1b and S1). Argon (c) and water (d) sorption isotherms are also given in Figure 1. The sorption isotherms show that the Co-ZIF-90 powder is porous. Analysis of the type I argon physisorption isotherm[54] results in a BET area of 750 m^2/g. No significant water adsorption occurs until a relative water pressure of 0.4. The main water uptake takes place at a relative pressure ranging between 0.4 and 0.55.

3.2. Characterization of the ZIF-8 Seeding Layer. ZIF-8 can be grown directly on substrates like glass and silicon at room temperature. We have modified the original synthesis recipe[35] and were able to improve the quality of the coatings, for example, by elucidating how to avoid cracks in the films.[49]

ZIF-8 thin films are grown by mixing methanolic solutions of the two precursors zinc nitrate hexahydrate and 2-methylimidazole in the presence of a substrate. This process can be repeated to grow thicker films (cycle-based method). As a result, crystalline and highly transparent thin films are obtained. XRD patterns of the resulting films that were synthesized on silicon wafers with one, and two deposition cycles are given in Figure 2. The reflections in the XRD pattern

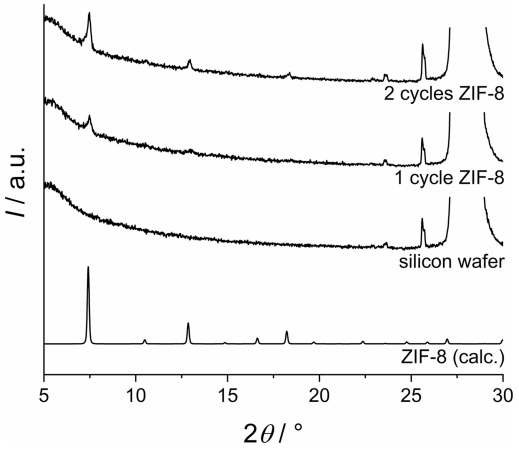

Figure 2. XRD patterns of ZIF-8 thin films on silicon substrates after one and two deposition cycles compared to the calculated XRD pattern of ZIF-8.[4] An XRD pattern of an uncoated silicon wafer is given as a reference.

of the coated substrates show a good agreement with the XRD pattern that can be calculated from the crystal structure of ZIF-8.[4] An uncoated silicon wafer is given as a reference. Additional signals can be seen especially at diffraction angles above 25° 2θ. These are caused by the substrate. Here and in the following, we have normalized the XRD pattern to the highest intensity between 5° and 10° 2θ because of the high intensity of the reflections that are caused by the silicon substrate.

Krypton physisorption measurements show that the thin films are porous after only one deposition cycle, as shown below (Section 3.4). The total uptake and the BET area both increase with the number of deposition cycles, as we have shown before.[49] SEM images of the films after one and two deposition cycles are given in the Supporting Information (Figure S2). No significant differences are visible for the two images. Both films are crack-free and dense. No voids or larger inhomogeneities are visible. Further characterizations of ZIF-8

https://doi.org/10.1021/acs.cgd.2c00664
Cryst. Growth Des. 2022, 22, 7008–7020

thin films (ellipsometry, UV/vis spectra, and AFM data) can be found in the Supporting Information (see Figures S3–S5). These experimental data indicate that a crystalline and porous ZIF-8 film can be formed after only one deposition cycle on silicon. ZIF-8 thin films will be used as seeding layers in the following subchapters. These seeding layers will be synthesized with only one deposition cycle, as the results presented here have shown that the quality of the thin films is sufficiently high already after one deposition cycle.

3.3. ZIF-8 Seeding Layers for MOF-on-MOF Coatings.

Attempts to transfer the synthesis method described above for ZIF-8 thin films to other ZIFs have usually not been successful. The Fischer group[48] has presented optimized synthesis conditions for some ZIF thin films, but as the aim of their study was not directed toward optical applications, the produced thin films do not possess the necessary optical quality. Nevertheless, we have employed some of the approaches described by the Fischer group,[48] like the use of different metal precursors (nitrates and acetates), different solvents (methanol and DMF), and of solvent mixtures. However, even by broad-ranging variations of the synthesis parameters, we were not able to obtain Co-ZIF-90 thin films of optical quality on silicon or glass. Typically, rough coatings of separated microcrystals were obtained, exhibiting strong light scattering. Thus, we shifted our focus from thin films that were directly grown on the substrate to ZIF-8-supported thin films.

In the following experiments, all Co-ZIF-90 films were grown on top of a ZIF-8 thin film that was prepared with one deposition cycle. These ZIF-8 seeding layers were synthesized in situ and were directly used without drying or storage.

First, the growth of Co-ZIF-90 with cobalt(II) nitrate as the only cobalt precursor was tested. No reflections are visible in the XRD pattern of such a sample (Figure 3). Also, no significant change in the UV/vis spectra before and after this synthesis can be seen (see Figure S6, Supporting Information). This indicates that no growth of Co-ZIF-90 takes place during the Co-ZIF-90 growth attempt. Therefore, we tested cobalt(II) acetate as an alternative cobalt source. However, when methanolic solutions of imidazole-2-carboxaldehyde ("HImCA") and cobalt(II) acetate are mixed, precipitation occurs immediately, resulting in the powder samples described in Section 3.1.

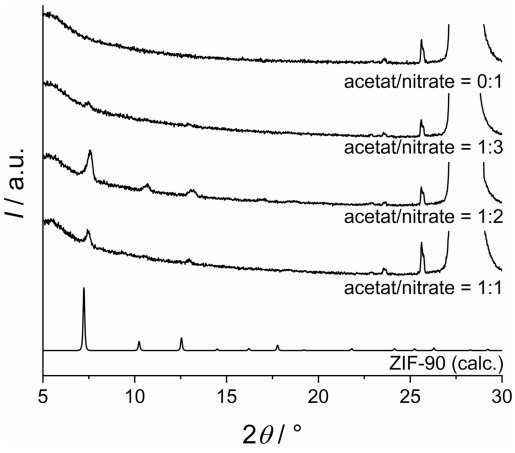

Figure 3. XRD patterns of MOF-on-MOF coatings of Co-ZIF-90 on a ZIF-8 seeding layer. All films were synthesized on silicon with two deposition cycles for the Co-ZIF-90 thin film. The influence of the cobalt precursors was investigated by mixing cobalt(II) nitrate and cobalt(II) acetate in different ratios. The reaction time for the Co-ZIF-90 deposition cycles was kept at 60 min per cycle. A calculated XRD pattern of ZIF-90 is given as a ref 52.

This could be explained with the basicity of the two anions: the pK_B values for acetate and nitrate are 9.25 (acetate) and 15.32 (nitrate). Hence, acetate is more alkaline in solution than nitrate and has a higher ability to deprotonate linker molecules. The linker deprotonation is an important step in the formation of a ZIF since the linkers are incorporated into the framework in their deprotonated form. The use of acetate thus leads to a higher supersaturation, which increases the rates of nucleation and growth.[55] Thus, when cobalt(II) acetate is used as the only cobalt source, formation of Co-ZIF-90 takes place immediately and throughout the solution. On the contrary, no crystallization is observed when cobalt(II) nitrate is the sole cobalt precursor, even after a few days. With the correct mixture of the two anions nitrate and acetate, the rate of the crystallization process can be fine-tuned so that the formation of Co-ZIF-90 can occur but is governed by heterogeneous nucleation and subsequent growth on the ZIF-8 seeding layer.

Therefore, we attempted to control the crystallization of Co-ZIF-90 from mixed solutions with different ratios of cobalt(II) nitrate to cobalt(II) acetate in the cobalt precursor solutions: the part of the acetate amounted to 25% (acetate/nitrate ratio of 1:3), 33.3% acetate (1:2), and 50% acetate (1:1), respectively. The XRD diffraction patterns of thin films that were grown with these solutions are given in Figure 3. The reaction time for all Co-ZIF-90 deposition cycles was kept at 60 min per cycle. It should be mentioned here that ZIF-8 and ZIF-90 show very similar reflections in their XRD diffraction patterns because both ZIFs crystallize in the **sod** topology with very similar cell parameters. Thus, we have to assess the degree of Co-ZIF-90 growth from intensity increases in the XRD patterns. The highest intensities of the reflections were found for an acetate to nitrate ratio of 1:2. Significantly lower intensities were obtained for higher and lower acetate concentrations (1:1 and 1:3). These results show that the ratio of acetate to nitrate in the cobalt precursor solution has a very strong influence on the Co-ZIF-90 growth. The ratio of different metal precursors, that is, of different anions, appears as an interesting novel synthesis parameter for the growth of ZIF thin films, especially when it is reconciled that syntheses with single component cobalt precursors do not work. Accordingly, the synthesis window for the preparation of Co-ZIF-90 thin films is very limited. A ratio of 1:2 (33.3% acetate) was kept for the following experiments.

The influence of the reaction time on Co-ZIF-90 film growth was investigated in the following experiments. XRD patterns of thin films that were grown with reaction times of 30, 45, and 60 min per cycle are given in Figure 4. The intensity of the reflections increases in comparison with the XRD diffraction pattern of the ZIF-8 seeding layer, indicating that Co-ZIF-90 films had grown (see Figure 2). Thus, at all tested reaction times, crystalline Co-ZIF-90 thin films were obtained, even after a short reaction time of 30 min per deposition cycle. Also, an increase of the intensities with increasing reaction time can be observed. This can be explained by the increased thickness of films that had been incubated for longer deposition times (see Figure S7, Supporting Information). The thicknesses were measured via ellipsometry and scale linearly in the investigated range (160

https://doi.org/10.1021/acs.cgd.2c00664
Cryst. Growth Des. 2022, 22, 7008−7020

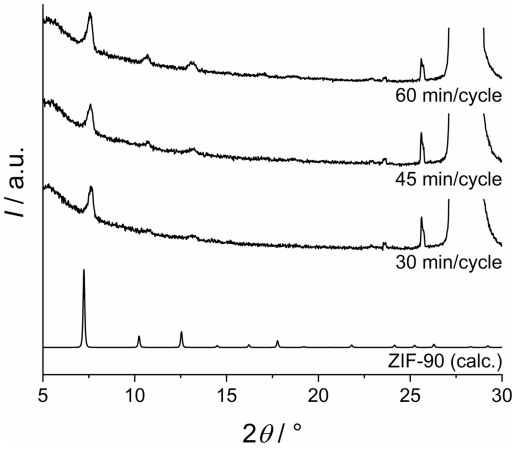

Figure 4. XRD patterns of Co-ZIF-90-on-ZIF-8 thin films on silicon substrates. The Co-ZIF-90 thin films were synthesized with two deposition cycles with different reaction times ranging from 30 to 60 min per cycle. A calculated XRD pattern of ZIF-90 is given as a ref 52.

nm thickness after 30 min, 245 nm after 45 min, and 310 nm after 60 min).

The quality of the Co-ZIF-90 coatings was first investigated using SEM (see Figure 5). Reaction times of 30 and 45 min per cycle yield thin films of good quality with only very few, very narrow cracks. Especially on the sample prepared with 30 min cycles, the cracks are hard to discern. On the contrary, when the deposition time was increased to 60 min per cycle, the sample shows a high number of considerably wider cracks. Thus, a reaction time of 45 min per cycle should not be exceeded to obtain high film quality. We used a reaction time of 30 min per cycle for the following experiments.

All previous experiments were conducted using a HImCA concentration of 50 mM. The influence of the linker concentration was investigated in the range between 40 and 75 mM, keeping the ratio of HImCA to the cobalt(II) precursors at 4:1—in consequence, concentrations of 10–18.75 mM were used for the mixed cobalt(II) solutions. XRD patterns of the resulting MOF-on-MOF coatings are shown in Figure 6. The intensities of the reflections increase with

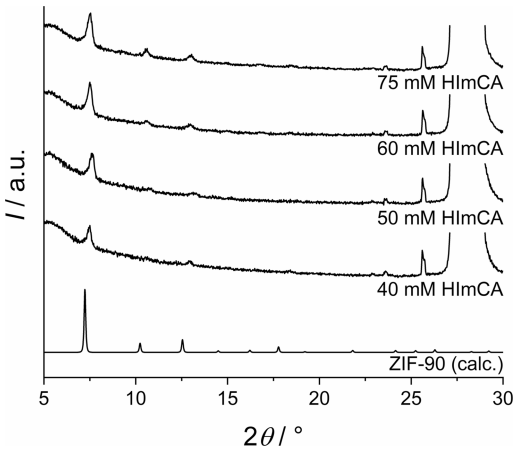

Figure 6. XRD patterns of MOF-on-MOF coatings on silicon substrates. The Co-ZIF-90 thin films were synthesized with two cycles of 30 min each with different precursor concentrations. The concentration of the linker (HImCA) is given for each pattern; the ratio of HImCA to cobalt(II) was kept at 1:4 for all syntheses. A calculated XRD pattern of ZIF-90 is given as a ref 52.

increasing concentration, indicating that higher precursor concentrations yield thicker Co-ZIF-90 films. Ellipsometry measurements confirm the increase of the thickness of the Co-ZIF-90 thin films at higher precursor concentrations (see Figure S8, Supporting Information). Crystalline thin films were obtained for all concentrations. Only for the film that was synthesized at the lowest linker concentration, the reflections exhibited considerably lower intensity. The ellipsometry results prove that only a thin layer with a thickness below 100 nm had grown at this concentration leading to the low intensity of these reflections.

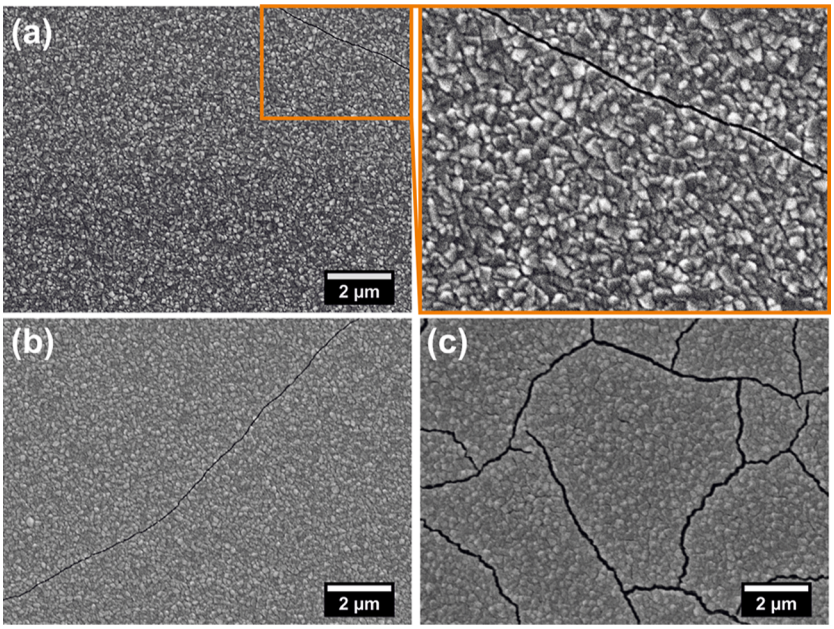

Figure 5. SEM images of Co-ZIF-90 thin films that were grown with reaction times of 30 min [(a)—with zoom-in to one of very few, very narrow cracks], 45 min (b), and 60 min (c) per cycle.

https://doi.org/10.1021/acs.cgd.2c00664
Cryst. Growth Des. 2022, 22, 7008−7020

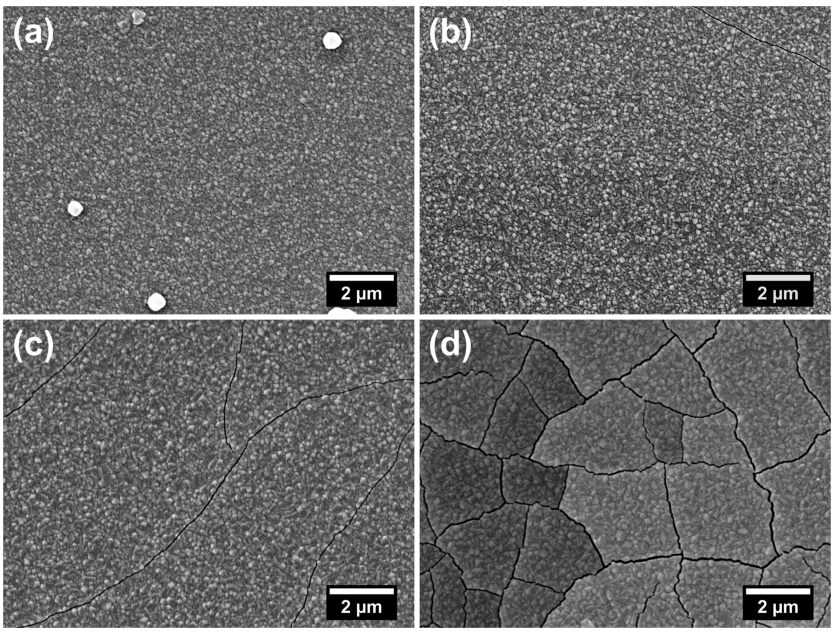

Figure 7. SEM images of Co-ZIF-90-on-ZIF-8 coatings. The Co-ZIF-90 thin films were synthesized with two deposition cycles with a reaction time of 30 min per cycle. The influence of the concentration of imidazole-2-carbaldehyde was investigated in the range from 40 to 75: (a) 40, (b) 50, (c) 60, and (d) 75 mM.

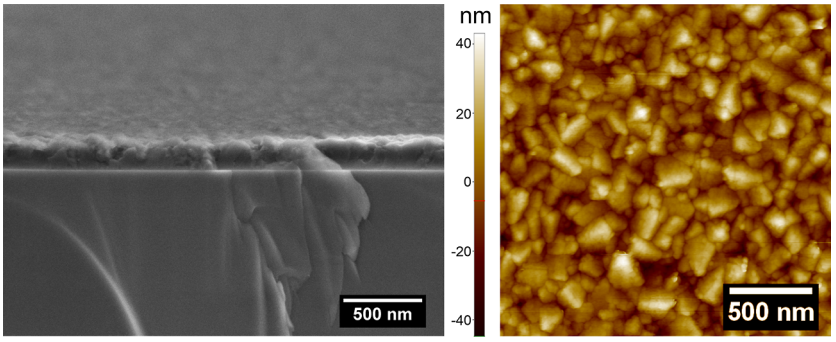

Figure 8. SEM cross-sectional image (left) and AFM topographical image (right) of the MOF-on-MOF thin film, consisting of ZIF-8 and Co-ZIF-90 (two deposition cycles).

The quality of the coatings was assessed by the SEM images, which are given in Figure 7. Two main influences of increasing precursor concentration can be seen: (i) the number of inhomogeneities (crystals that grow on the surface of the film) decreases and (ii) the number of cracks and their width increase. Cracks first appear at a concentration of 50 mM, but these are small in number and narrow. Also, larger areas of the films are crack-free, so that the optical quality of these films is good. Increasing the concentration to 75 mM results in films that have a large number of cracks that are evenly distributed over the sample. The large number of cracks reduces the quality of the films. Since inhomogeneities can cause scattering and are therefore more problematic than narrow cracks, we chose to conduct the optical characterizations on Co-ZIF-90 coatings that were prepared at a precursor concentration of 50 mM HImCA. Only two deposition cycles are needed for Co-ZIF-90 to obtain a thin film with a thickness of around 150 nm on top of a ZIF-8 thin film with a thickness of around 80 nm. The total synthesis time to grow this system is 90 min, so the growth is very fast compared to other procedures yielding MOF-on-MOF coatings, which were described in the introduction.

The homogeneity of the film was also investigated using SEM cross-sectional images (see Figure 8, left, and Figure S9 in the Supporting Information) and AFM (example image in Figure 8, right). Both films (ZIF-8 seeding layer and Co-ZIF-90 film) are intergrown very well. No separation of the films is visible at the interface between the two ZIFs. According to the SEM images, a total film thickness of 200−250 nm is found, which is in good agreement with the ellipsometry result on the same films (220 nm). The films are homogeneous over large areas from the cross-sectional view. An analysis of the heights of the pixels in the AFM topographical images results in a roughness of R_a = 9.0 ± 0.6 nm. The roughness is slightly increased in comparison with the ZIF-8 seeding layer (R_a = 5.4 ± 0.5) but still reflects a nearly smooth surface.

The MOF-on-MOF film of Co-ZIF-90 on ZIF-8 on silicon substrates was further investigated using two sensitive methods, ellipsometry and XPS. In an ellipsometry measurement, the amplitude ratio Ψ and the phase difference Δ are measured in a chosen wavelength range. Afterward, a model has to be chosen for the fitting of the data. Values for the refractive index (n), the absorption (k), and the thickness (d) of every film are fitted by the software according to this model.

https://doi.org/10.1021/acs.cgd.2c00664
Cryst. Growth Des. 2022, 22, 7008−7020

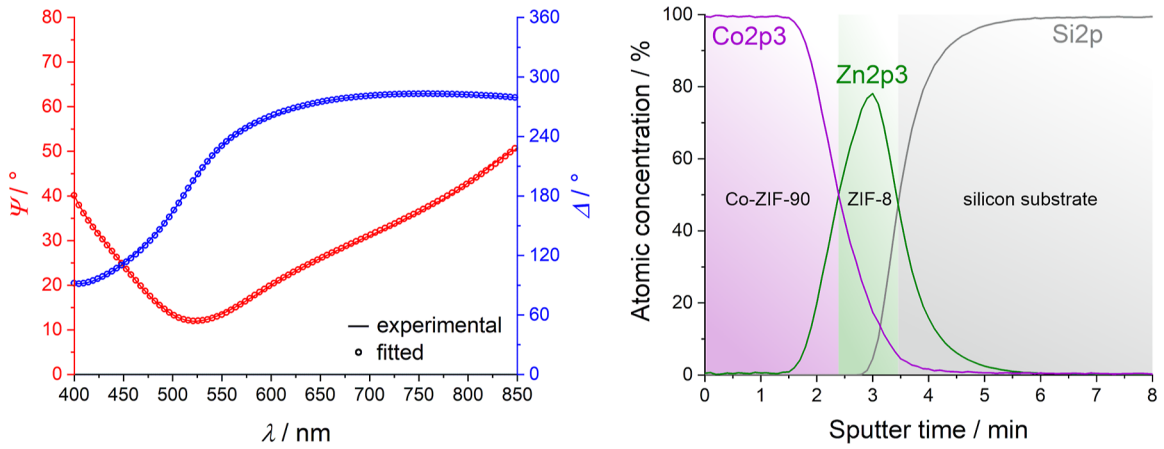

Figure 9. Results from ellipsometry and XPS obtained on Co-ZIF-90-on-ZIF-8 coatings (two deposition cycles for Co-ZIF-90 on a ZIF-8 seeding layer). Left: plot of the experimental and fitted data from the ellipsometry measurement. Right: depth profile of the atomic concentrations on the sample surface measured by XPS, given as a function of the sputtering time.

The quality of the fit, which strongly depends on the chosen model, can be observed by comparing the experimental curves for Ψ and Δ with the fitted ones. A typical result is given in Figure 9 (left): the agreement between the experimental (lines) and the fitted data (dots) is very good. The fit has a low mean squared error (MSE) of 0.5, which underlines the good agreement. Details about the used ellipsometry model and the set values are given in Table S1, accompanied by explanatory text, in the Supporting Information. The refractive index of Co-ZIF-90 at 589 nm is 1.457 with an absorption maximum at 552 nm. According to the fit, the total thickness of the MOF-on-MOF coating is 232.5 nm.

Using XPS, we measured depth profiles of a MOF-on-MOF coating. In these experiments, the surface is treated with an argon cluster ion beam that removes the surface of the sample in a time-controlled sputtering process. Sputtering was performed for 6 s each, followed by an XPS measurement. This process of sputtering and measurements was repeated until no MOF film was present anymore. The resulting atomic concentrations as a function of sputtering time are shown in Figure 9 (right) for cobalt (from Co-ZIF-90), zinc (from ZIF-8), and silicon (from the silicon wafer which was used as the substrate). No significant signal for zinc and silicon is present in the beginning of the experiment. According to this, Co-ZIF-90 forms a dense coating on top of the ZIF-8 seeding layer. After ca. 2 min of sputtering, a decrease of the cobalt concentration can be detected. The atomic concentration of zinc increases at the same time. By further removing the surface during sputtering, the cobalt signal further decreases, whereas the zinc signal passes through a maximum. After 6 minutes, no more signals for cobalt and zinc can be detected, whereas the atomic concentration of silicon increases to 100%, showing that the MOF thin films were completely removed from the silicon surface. Although it is not easy to give quantitative data for the thicknesses of the individual film, it is obvious that the Co-ZIF-90 part of the total deposited is considerably larger than that of ZIF-8.

Accessible porosity is a major property of MOFs important for many applications. In Figure 10, two krypton physisorption isotherms are shown: one of the ZIF-8 seeding layer (one deposition cycle) and one of the MOF-on-MOF coating, both synthesized on silicon wafers. Both diagrams show type I isotherms typical of microporous materials.[54] An increase of

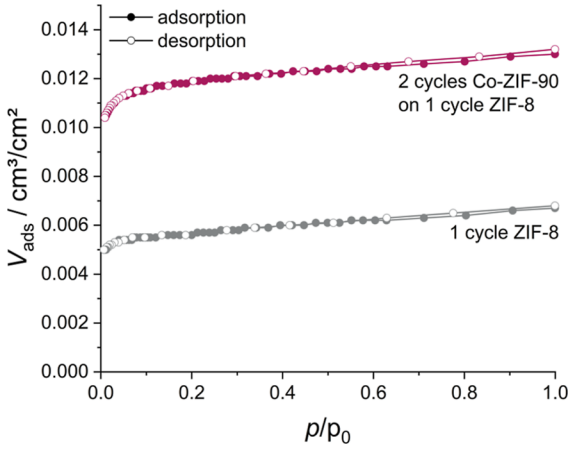

Figure 10. Krypton physisorption isotherms of the ZIF-8 seeding layer (one deposition cycle) and of the MOF-on-MOF coating (one cycle ZIF-8 and two cycles Co-ZIF-90).

the total uptake can be seen when Co-ZIF-90 is coated on top of the ZIF-8 seeding layer. From the BET analysis on both isotherms, an increase of the BET area from 250 cm^2/cm^2 for the ZIF-8 seeding layer to 470 cm^2/cm^2 for the MOF-on-MOF coating is found, verifying that the Co-ZIF-90 film is porous and both layers of the coating can be accessed by krypton gas.

We also studied the deposition of Co-ZIF-90-on-ZIF-8 MOF-on-MOF coatings on glass substrates. Photographies of Co-ZIF-90 thin films that were synthesized on glass substrates with two, four, and six deposition cycles are given in Figure 11. Uncoated glass and ZIF-8-coated glass are given as a reference. XRD patterns of the samples prepared with different numbers of Co-ZIF-90 deposition cycles are given in the Supporting Information (Figure S10), confirming that the films are also crystalline when the synthesis is performed on glass instead of silicon. All coatings with Co-ZIF-90 layers have a purple color, which is homogeneous over the whole samples and which intensifies with increasing number of deposition cycles. The samples are highly transparent to the naked eye. No turbidity or scattering can be seen.

The results presented in this subchapter show that we have been able to optimize the synthesis conditions for the growth of a Co-ZIF-90 thin film on ZIF-8-coated silicon or glass substrates. An important factor for the success of the synthesis

https://doi.org/10.1021/acs.cgd.2c00664
Cryst. Growth Des. 2022, 22, 7008−7020

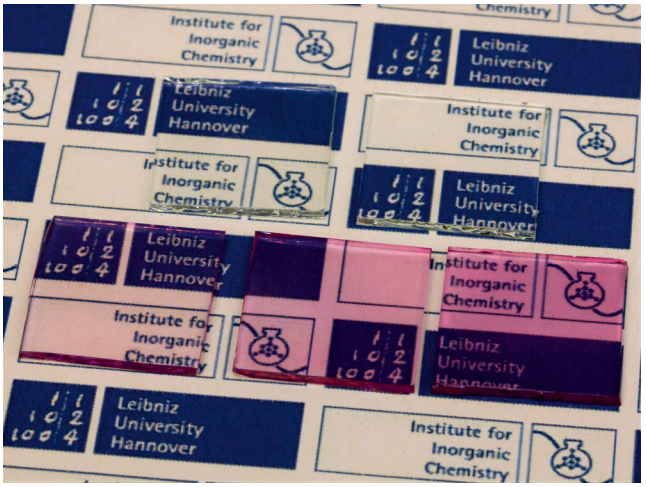

Figure 11. Photography of MOF-on-MOF coatings, which were synthesized with two, four, and six Co-ZIF-90 deposition cycles (bottom, from left to right). Uncoated glass (top left) and a glass slide with the ZIF-8 seeding layer only (top right) are shown for comparison. Copyright for use of the logos of the Leibniz University Hannover and the Institute for Inorganic Chemistry was permitted.

lies in the adaptation of the types of precursors and their concentrations. These strongly influence the formation of cracks or other inhomogeneities. The crystallization of high-quality optical coatings was enabled by mixing one part of cobalt(II) acetate and two parts of cobalt(II) nitrate as cobalt precursors. Optimal concentrations are 50 mM for the imidazole-2-carbaldehyde and 12.5 mM for the cobalt solution. Nearly no cracks were obtained at these concentrations. With short reaction times of 30 min per cycle (longer reaction times result in films with larger cracks), the total synthesis time for a MOF-on-MOF coating amounts to only 90 min.

3.4. Optical Characterization. In order for an optical material to function in an optical device, it should be fabricated in a shape and a quality which allows for the incoupling, transmission, or outcoupling of light. Thin films are a suitable morphology for many applications, but they need to be of optical quality. Therefore, the following properties should be given: the films should provide a high transparency and a high homogeneity as well as none or only very few scattering centers. Scattering occurs when materials with two different refractive indices are present and when their dimensions are similar to the wavelengths of light. Especially large refractive index differences occur when one of the materials is air (or vacuum). In thin films, this relates to the outer boundary of the thin film—so the films should be smooth—and to voids within the film—so the films should be dense. Voids within a film are an example for scattering centers and may appear as interparticle gaps (typical of films obtained by nanoparticle deposition) or as cracks (often forming in directly grown films during drying or as a consequence of temperature changes). Also, additional deposits of foreign substances (either within the film or on its surface) can act as scattering centers, although the refractive index difference is smaller then. With regard to thin films of MOFs, we expect in addition that they feature an addressable porosity which may, for example, be used in sensors[56,57] or to manipulate the refractive index.[33,49] Preferably, the films should be crystalline, with the defined structure enhancing, for example, the selectivity in sensing.

We have shown that our Co-ZIF-90 thin films are crystalline and nanoporous. Also, they are homogeneous and void-free as well as rather smooth; in addition, when prepared under optimized conditions, they possess only very few very narrow cracks. Therefore, they are well-suited to further explore their optical properties and functionalities.

Important optical properties of the thin films are their light transmission characteristics and their refractive index. The UV/vis transmission spectrum of a Co-ZIF-90-on-ZIF-8 coating on glass (two deposition cycles for Co-ZIF-90) in an argon atmosphere is given in Figure 12. A high transmission of

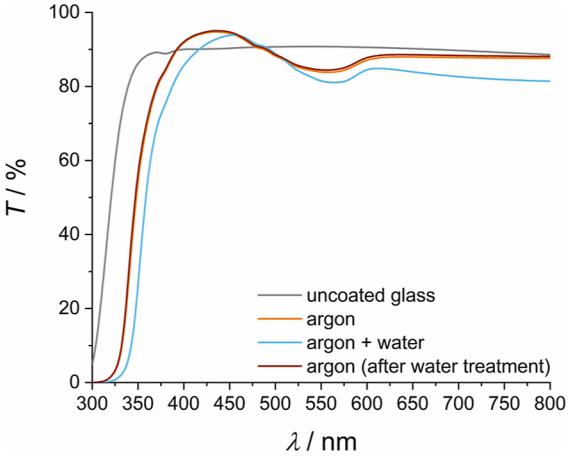

Figure 12. UV/vis transmission spectra of Co-ZIF-90-on-ZIF-8 coatings on glass substrates, synthesized with two deposition cycles for Co-ZIF-90. The transmission is given for samples in an argon atmosphere (orange line), in moist argon (blue line), and again in argon after the water treatment (red line). The transmission of the blank glass slide substrate is given as a reference.

at least 80% is given above 370 nm. Absorption can be observed between 500 and 600 nm with a maximum at 558 nm, which is in good agreement with the ellipsometry measurement that is discussed in Section 3.4. This absorption in the area of the yellow light is reflected by the purple color of the samples. An increased absorption is observed in the near UV, resulting in a lower transmission compared to glass below 400 nm. Nearly no transmission difference between the coated and uncoated glasses can be seen in the red and near IR range of the light spectrum. The films provide a high quality especially in this range of the light spectrum. When the samples are exposed to humidity, a shift of the spectrum can be observed. The transmission through the films decreases, but a transmission of at least 80% is still given above 390 nm. The absorption maximum shifts to 565 nm. This shift is reversible when the films are exposed to dry argon again. The highest transmission differences can be found at the border to the UV region between 325 and 400 nm. A shift in the transmission spectrum corresponds to a change in the optical properties of the thin films and should also be visible for other optical properties like the refractive index of the MOF films.

We investigated the refractive index of the Co-ZIF-90 thin films in atmospheres with controlled RH using ellipsometry. This was performed in a static experiment, so the films were left in the atmosphere with the predefined RH for a few minutes before the ellipsometry measurements were taken in eightfold replication. The refractive index dispersion curves were averaged for each RH value. Figure 13 shows the

https://doi.org/10.1021/acs.cgd.2c00664
Cryst. Growth Des. 2022, 22, 7008−7020

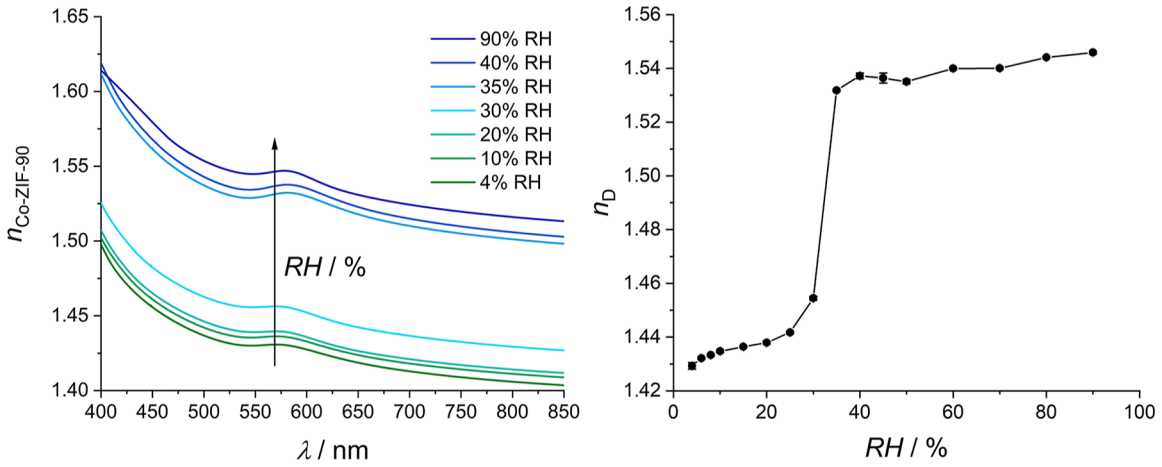

Figure 13. Left: refractive index dispersion curves of Co-ZIF-90 thin films at a different RH ranging from 4 to 90% RH. Right: a plot of the resulting refractive indices at 589 nm (n_D) as a function of RH.

averaged refractive index dispersion curves at different RH (left graph) and the refractive index at 589 nm (n_D, D line of sodium vapor) for different RH values. For a better overview, not all of the refractive index dispersion curves are shown in this graph. The dispersion curves measured at all investigated RH values are given in Figure S11. As usual, the refractive index dispersion curves globally show a decay with increasing wavelength. The observed increase of the refractive index around 575 nm is found for all samples. It is caused by the absorption of the yellow light in this wavelength range and is expected for a purple-colored material. An absorption in this range also appears in the UV/vis spectrum of a Co-ZIF-90-on ZIF-8 coating on glass, which is shown in Figure 12. In our ellipsometry experiments, the lowest RH is 4%, and the highest is 90%. In the range from 4 to 20% RH, only a small increase of the refractive index is visible. A pronounced increase of the refractive index can be observed between 20 and 40% RH with the largest change of Δn_D = 0.07 between 30 and 35% RH (Figure 13, right). In total, a refractive index increase of Δn_D = 0.10 takes place between 20 and 40% RH. At higher humidity, the refractive index stabilizes between 40 and 90% RH and shows no further significant increase. A similar behavior is also found for the Co-ZIF-90 particles in water vapor sorption experiments. These exhibit a pronounced water uptake step at a relative pressure between 0.4 and 0.55 (see Figure 1). The difference in the positions of the water uptake step on the RH versus the relative pressure scale can be explained by the different experimental approaches and specifically by the medium of the water vapor: water in argon for the ellipsometry measurements on the thin films and vacuum for the water sorption measurements on the powder.

The reversibility of the refractive index modulation upon exposure of the thin films to different RHs was investigated using ellipsometry. The refractive index was measured while the RH was alternated between 10 and 60% RH in cycles showing a high reversibility (see Figure S12 in the Supporting Information). This experiment still shows the static refractive index modulation and is not time-resolved, since the ellipsometry measurements take around 15 s per measurement. The rate of the refractive index change caused by humidity was investigated in a UV/vis kinetic measurement that is described in detail in the Supporting Information. A home-built measurement cell with quartz glass windows and an inlet and outlet for gases was used. The transmission through a Co-ZIF-90-on-ZIF-8-coated glass slide was automatically measured every 0.1 s at a wavelength of 350 nm. This wavelength was chosen because the films have the highest transmission difference between the dry state (in argon) and the moist state (in humidified argon) here. Figure 14 shows the

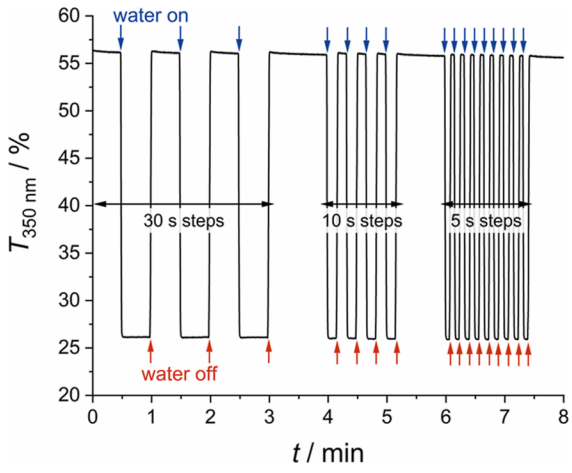

Figure 14. UV/vis kinetic experiment on a Co-ZIF-90-on-ZIF-8-coated glass slide in dry and moist argon atmosphere. Different time steps were employed for the switching between dry and moist argons. The transmission was measured at 350 nm with a resolution of 0.1 s.

evolution of the transmission in this time-resolved experiment. Arrows indicate changes between the dry and moist atmosphere. A complete recovery of the transmission is achieved even for the fastest switching times of 5 s showing that the adsorption and desorption of water in the films take place very fast. A reference experiment that was performed on a ZIF-8-coated glass slide is given in Figure S13 (Supporting Information). Also, further explanations on this experiment can be found in the Supporting Information. Nearly no transmission changes are visible for the ZIF-8 thin films when the atmosphere is switched from dry to moist or reverse. Hence, the ZIF-8 seeding layer has no impact on the switching behavior of the Co-ZIF-90-on-ZIF-8 coating. Since the changes in the transmission and the refractive index are related with each other,[35] we can say that the switching of the refractive index takes place on the second time scale. A detailed

https://doi.org/10.1021/acs.cgd.2c00664
Cryst. Growth Des. 2022, 22, 7008−7020

analysis of the switching times in the "5 s steps" is shown in Figure S14. The transmission was normalized for this analysis with the transmission in dry argon atmosphere being 100% and the transmission in moist argon atmosphere being 0%. We analyzed the time difference between the beginning of the transmission decay of the signal and the time, where 90% of this decay is completed. Based on this evaluation, we can say that the water sorption takes around 1 s. An analogously performed analysis for the water desorption results in a desorption time of around 1.5 s.

4. CONCLUSIONS

We have reported the synthesis of thin films of the cobalt version of ZIF-90 (Co-ZIF-90) that can be grown at room temperature using a cycle-based growth method. This method enables a fast growth of the thin films within 90 min. High-quality ZIF-8 thin films were used as seeding layers to enable the growth of the Co-ZIF-90 thin films as a MOF-on-MOF coating. We have shown how the different synthesis parameters influence the quality of the thin films in terms of crystallinity and optical quality. Co-ZIF-90 cannot be grown from solutions containing only cobalt(II) nitrate or acetate since either no growth of the MOF is observed or a very fast crystallization takes place directly after mixing the precursor solutions. Mixing the nitrate and acetate in different ratios enables the control over the growth of the MOF, which is key to grow the thin films. We have optimized the concentration range, the acetate to nitrate ratio, and the reaction times and have obtained nearly crack-free Co-ZIF-90-on-ZIF-8 coatings of optical quality. The films provide a high transparency and are highly crystalline and porous. Two aspects of our investigation on the preparation of the Co-ZIF-90 thin films can be considered as promising novel approaches to control the growth of MOF thin films (or other morphologies of MOFs): (i) the use of a high quality seeding layer of one MOF to enable the direct growth of another MOF and (ii) the use of a mixture of salts of the same metal with different anions as precursor.

We have investigated the refractive index of the thin films in detail. The films show a high affinity toward water above a certain RH that results in a strong refractive index change with a jump of the refractive index between 30 and 35% RH. In total, a refractive index change of $\Delta n \approx 0.1$ was achieved by changing from dry to moist argon and reverse. Further ellipsometry measurements and a UV/vis kinetic study showed the high reversibility of the refractive index modulation that takes place very fast, with a switching time on the time scale of 1 s. Alternation between dry and moist argon can be resolved well even at a fast alternation time of 5 s.

Basically, this study shows that by using novel concepts (seeding layer) and by studying reaction conditions in depth, the generation of thin films of optical quality from novel materials using cycled direct growth becomes possible. Cycled direct growth yields high quality films considerably faster than traditional LPE growth techniques for MOF thin films.

ASSOCIATED CONTENT

Supporting Information

The Supporting Information is available free of charge at https://pubs.acs.org/doi/10.1021/acs.cgd.2c00664.

Evaluation of the ellipsometry data, characterization of the Co-ZIF-90 powder samples, the ZIF-8 seeding layer, and Co-ZIF-90-on-ZIF-8 coatings, optical characterization of the Co-ZIF-90-on-ZIF-8 coatings, and the UV/vis kinetic experiments (PDF)

AUTHOR INFORMATION

Corresponding Author

Peter Behrens − *Institute of Inorganic Chemistry, Leibniz University Hannover, Hannover 30167, Germany; Cluster of Excellence PhoenixD (Photonics, Optics and Engineering—Innovation Across Disciplines), Leibniz University Hannover, Hannover 30167, Germany*; Email: peter.behrens@acb.uni-hannover.de

Authors

Nils Christian Keppler − *Institute of Inorganic Chemistry, Leibniz University Hannover, Hannover 30167, Germany; Cluster of Excellence PhoenixD (Photonics, Optics and Engineering—Innovation Across Disciplines), Leibniz University Hannover, Hannover 30167, Germany;* orcid.org/0000-0002-3133-3014

Johanna Fricke − *Institute of Inorganic Chemistry, Leibniz University Hannover, Hannover 30167, Germany*

Andreas Schaate − *Institute of Inorganic Chemistry, Leibniz University Hannover, Hannover 30167, Germany; Cluster of Excellence PhoenixD (Photonics, Optics and Engineering—Innovation Across Disciplines), Leibniz University Hannover, Hannover 30167, Germany;* orcid.org/0000-0001-7908-6553

Adrian Hannebauer − *Institute of Inorganic Chemistry, Leibniz University Hannover, Hannover 30167, Germany*

Karen Deli Josephine Hindricks − *Institute of Inorganic Chemistry, Leibniz University Hannover, Hannover 30167, Germany; Cluster of Excellence PhoenixD (Photonics, Optics and Engineering—Innovation Across Disciplines), Leibniz University Hannover, Hannover 30167, Germany;* orcid.org/0000-0002-5549-922X

Saskia Zailskas − *Institute of Inorganic Chemistry, Leibniz University Hannover, Hannover 30167, Germany*

Complete contact information is available at: https://pubs.acs.org/10.1021/acs.cgd.2c00664

Notes

The authors declare no competing financial interest.

ACKNOWLEDGMENTS

This work was funded by the Deutsche Forschungsgemeinschaft (DFG) under Germany's Excellence Strategy within the Cluster of Excellence PhoenixD (EXC 2122, Project ID 390833453). Karen Hindricks thanks the Studienstiftung des Deutschen Volkes (German National Academic Foundation) for a scholarship. Adrian Hannebauer thanks the HSN (Hannover School for Nanotechnology) for a scholarship. We thank Younes Senft for building the UV/vis measurement cell.

REFERENCES

(1) Panella, B.; Hirscher, M. Hydrogen Physisorption in Metal-Organic Porous Crystals. *Adv. Mater.* **2005**, *17*, 538−541.

(2) Cavka, J. H.; Jakobsen, S.; Olsbye, U.; Guillou, N.; Lamberti, C.; Bordiga, S.; Lillerud, K. P. A new zirconium inorganic building brick forming metal organic frameworks with exceptional stability. *J. Am. Chem. Soc.* **2008**, *130*, 13850−13851.

(3) Chui, S. S.-Y.; Lo, S. M.-F.; Charmant, J. P. H.; Orpen, A. G.; Williams, I. D. A Chemically Functionalizable Nanoporous Material $[Cu_3(TMA)_2(H_2O)_3]_n$. *Science* **1999**, *283*, 1148−1150.
(4) Park, K. S.; Ni, Z.; Côté, A. P.; Choi, J. Y.; Huang, R.; Uribe-Romo, F. J.; Chae, H. K.; O'Keeffe, M.; Yaghi, O. M. Exceptional chemical and thermal stability of zeolitic imidazolate frameworks. *Proc. Natl. Acad. Sci. U.S.A.* **2006**, *103*, 10186−10191.
(5) Rosi, N. L.; Kim, J.; Eddaoudi, M.; Chen, B.; O'Keeffe, M.; Yaghi, O. M. Rod packings and metal-organic frameworks constructed from rod-shaped secondary building units. *J. Am. Chem. Soc.* **2005**, *127*, 1504−1518.
(6) Grünker, R.; Bon, V.; Müller, P.; Stoeck, U.; Krause, S.; Mueller, U.; Senkovska, I.; Kaskel, S. A new metal-organic framework with ultra-high surface area. *Chem. Commun.* **2014**, *50*, 3450−3452.
(7) Gygi, D.; Bloch, E. D.; Mason, J. A.; Hudson, M. R.; Gonzalez, M. I.; Siegelman, R. L.; Darwish, T. A.; Queen, W. L.; Brown, C. M.; Long, J. R. Hydrogen Storage in the Expanded Pore Metal−Organic Frameworks M_2(dobpdc) (M = Mg, Mn, Fe, Co, Ni, Zn). *Chem. Mater.* **2016**, *28*, 1128−1138.
(8) Ji, Y.; Ding, L.; Cheng, Y.; Zhou, H.; Yang, S.; Li, F.; Li, Y. Understanding the Effect of Ligands on C_2H_2 Storage and C_2H_2/CH_4, C_2H_2/CO_2 Separation in Metal−Organic Frameworks with Open Cu(II) Sites. *J. Phys. Chem. C* **2017**, *121*, 24104−24113.
(9) Yang, X.; Xu, Q. Bimetallic Metal−Organic Frameworks for Gas Storage and Separation. *Cryst. Growth Des.* **2017**, *17*, 1450−1455.
(10) Böhme, U.; Barth, B.; Paula, C.; Kuhnt, A.; Schwieger, W.; Mundstock, A.; Caro, J.; Hartmann, M. Ethene/ethane and propene/propane separation via the olefin and paraffin selective metal-organic framework adsorbents CPO-27 and ZIF-8. *Langmuir* **2013**, *29*, 8592−8600.
(11) Fan, L.; Kang, Z.; Shen, Y.; Wang, S.; Zhao, H.; Sun, H.; Hu, X.; Sun, H.; Wang, R.; Sun, D. Mixed Matrix Membranes Based on Metal−Organic Frameworks with Tunable Pore Size for CO_2 Separation. *Cryst. Growth Des.* **2018**, *18*, 4365−4371.
(12) Knebel, A.; Geppert, B.; Volgmann, K.; Kolokolov, D. I.; Stepanov, A. G.; Twiefel, J.; Heitjans, P.; Volkmer, D.; Caro, J. Defibrillation of soft porous metal-organic frameworks with electric fields. *Science* **2017**, *358*, 347−351.
(13) Woellner, M.; Hausdorf, S.; Klein, N.; Mueller, P.; Smith, M. W.; Kaskel, S. Adsorption and Detection of Hazardous Trace Gases by Metal-Organic Frameworks. *Adv. Mater.* **2018**, *30*, 1704679.
(14) Allendorf, M. D.; Dong, R.; Feng, X.; Kaskel, S.; Matoga, D.; Stavila, V. Electronic Devices Using Open Framework Materials. *Chem. Rev.* **2020**, *120*, 8581−8640.
(15) Chughtai, A. H.; Ahmad, N.; Younus, H. A.; Laypkov, A.; Verpoort, F. Metal-organic frameworks: versatile heterogeneous catalysts for efficient catalytic organic transformations. *Chem. Soc. Rev.* **2015**, *44*, 6804−6849.
(16) Trickett, C. A.; Helal, A.; Al-Maythalony, B. A.; Yamani, Z. H.; Cordova, K. E.; Yaghi, O. M. The chemistry of metal−organic frameworks for CO_2 capture, regeneration and conversion. *Nat. Rev. Mater.* **2017**, *2*, 17045.
(17) Ge, X.; Wong, R.; Anisa, A.; Ma, S. Recent development of metal-organic framework nanocomposites for biomedical applications. *Biomaterials* **2022**, *281*, 121322.
(18) Wuttke, S.; Zimpel, A.; Bein, T.; Braig, S.; Stoiber, K.; Vollmar, A.; Müller, D.; Haastert-Talini, K.; Schaeske, J.; Stiesch, M.; Zahn, G.; Mohmeyer, A.; Behrens, P.; Eickelberg, O.; Bölükbas, D. A.; Meiners, S. Validating Metal-Organic Framework Nanoparticles for Their Nanosafety in Diverse Biomedical Applications. *Adv. Healthcare Mater.* **2017**, *6*, 1600818.
(19) Yang, J.; Yang, Y.-W. Metal-Organic Frameworks for Biomedical Applications. *Small* **2020**, *16*, 1906846.
(20) Shekhah, O.; Liu, J.; Fischer, R. A.; Wöll, C. MOF thin films: existing and future applications. *Chem. Soc. Rev.* **2011**, *40*, 1081−1106.
(21) Stassen, I.; Burtch, N.; Talin, A.; Falcaro, P.; Allendorf, M.; Ameloot, R. An updated roadmap for the integration of metal-organic frameworks with electronic devices and chemical sensors. *Chem. Soc. Rev.* **2017**, *46*, 3185−3241.
(22) Olorunyomi, J. F.; Geh, S. T.; Caruso, R. A.; Doherty, C. M. Metal-organic frameworks for chemical sensing devices. *Mater. Horiz.* **2021**, *8*, 2387−2419.
(23) Gu, Z.-G.; Pfriem, A.; Hamsch, S.; Breitwieser, H.; Wohlgemuth, J.; Heinke, L.; Gliemann, H.; Wöll, C. Transparent films of metal-organic frameworks for optical applications. *Microporous Mesoporous Mater.* **2015**, *211*, 82−87.
(24) Liu, X.-M.; Xie, L.-H.; Wu, Y. Recent advances in the shaping of metal−organic frameworks. *Inorg. Chem. Front.* **2020**, *7*, 2840−2866.
(25) Valizadeh, B.; Nguyen, T. N.; Stylianou, K. C. Shape engineering of metal−organic frameworks. *Polyhedron* **2018**, *145*, 1−15.
(26) Brown, A. J.; Johnson, J. R.; Lydon, M. E.; Koros, W. J.; Jones, C. W.; Nair, S. Continuous polycrystalline zeolitic imidazolate framework-90 membranes on polymeric hollow fibers. *Angew. Chem.* **2012**, *124*, 10767−10770.
(27) Kim, K.-J.; Lu, P.; Culp, J. T.; Ohodnicki, P. R. Metal-Organic Framework Thin Film Coated Optical Fiber Sensors: A Novel Waveguide-Based Chemical Sensing Platform. *ACS Sens.* **2018**, *3*, 386−394.
(28) Zhang, W.; Cai, G.; Wu, R.; He, Z.; Yao, H.-B.; Jiang, H.-L.; Yu, S.-H. Templating Synthesis of Metal-Organic Framework Nanofiber Aerogels and Their Derived Hollow Porous Carbon Nanofibers for Energy Storage and Conversion. *Small* **2021**, *17*, 2004140.
(29) Huang, A.; Dou, W.; Caro, J. Steam-stable zeolitic imidazolate framework ZIF-90 membrane with hydrogen selectivity through covalent functionalization. *J. Am. Chem. Soc.* **2010**, *132*, 15562−15564.
(30) Lee, D.-J.; Li, Q.; Kim, H.; Lee, K. Preparation of Ni-MOF-74 membrane for CO_2 separation by layer-by-layer seeding technique. *Microporous Mesoporous Mater.* **2012**, *163*, 169−177.
(31) Zhang, W.; Xu, C.-H.; Zheng, H.; Li, R.; Zhou, K. Oxygen-Rich Cobalt−Nitrogen−Carbon Porous Nanosheets for Bifunctional Oxygen Electrocatalysis. *Adv. Funct. Mater.* **2022**, *32*, 2200763.
(32) Cai, G.; Yin, Y.; Xia, D.; Chen, A. A.; Holoubek, J.; Scharf, J.; Yang, Y.; Koh, K. H.; Li, M.; Davies, D. M.; Mayer, M.; Han, T. H.; Meng, Y. S.; Pascal, T. A.; Chen, Z. Sub-nanometer confinement enables facile condensation of gas electrolyte for low-temperature batteries. *Nat. Commun.* **2021**, *12*, 3395.
(33) Redel, E.; Wang, Z.; Walheim, S.; Liu, J.; Gliemann, H.; Wöll, C. On the dielectric and optical properties of surface-anchored metal-organic frameworks: A study on epitaxially grown thin films. *Appl. Phys. Lett.* **2013**, *103*, 091903.
(34) Wang, Z.; Rodewald, K.; Medishetty, R.; Rieger, B.; Fischer, R. A. Control of Water Content for Enhancing the Quality of Copper Paddle-Wheel-Based Metal−Organic Framework Thin Films Grown by Layer-by-Layer Liquid-Phase Epitaxy. *Cryst. Growth Des.* **2018**, *18*, 7451−7459.
(35) Lu, G.; Hupp, J. T. Metal-organic frameworks as sensors: a ZIF-8 based Fabry-Pérot device as a selective sensor for chemical vapors and gases. *J. Am. Chem. Soc.* **2010**, *132*, 7832−7833.
(36) Phan, A.; Doonan, C. J.; Uribe-Romo, F. J.; Knobler, C. B.; O'Keeffe, M.; Yaghi, O. M. Synthesis, structure, and carbon dioxide capture properties of zeolitic imidazolate frameworks. *Acc. Chem. Res.* **2010**, *43*, 58−67.
(37) Shekhah, O.; Wang, H.; Kowarik, S.; Schreiber, F.; Paulus, M.; Tolan, M.; Sternemann, C.; Evers, F.; Zacher, D.; Fischer, R. A.; Wöll, C. Step-by-step route for the synthesis of metal-organic frameworks. *J. Am. Chem. Soc.* **2007**, *129*, 15118−15119.
(38) Chernikova, V.; Shekhah, O.; Eddaoudi, M. Advanced Fabrication Method for the Preparation of MOF Thin Films: Liquid-Phase Epitaxy Approach Meets Spin Coating Method. *ACS Appl. Mater. Interfaces* **2016**, *8*, 20459−20464.
(39) Müller, K.; Fink, K.; Schöttner, L.; Koenig, M.; Heinke, L.; Wöll, C. Defects as Color Centers: The Apparent Color of Metal-Organic Frameworks Containing Cu2+-Based Paddle-Wheel Units. *ACS Appl. Mater. Interfaces* **2017**, *9*, 37463−37467.

https://doi.org/10.1021/acs.cgd.2c00664
Cryst. Growth Des. 2022, 22, 7008−7020

(40) Miyamoto, M.; Kohmura, S.; Iwatsuka, H.; Oumi, Y.; Uemiya, S. In situ solvothermal growth of highly oriented Zr-based metal organic framework UiO-66 film with monocrystalline layer. *CrystEngComm* **2015**, *17*, 3422−3425.
(41) Huang, Y.; Tao, C.; Chen, R.; Sheng, L.; Wang, J. Comparison of Fabrication Methods of Metal-Organic Framework Optical Thin Films. *Nanomaterials* **2018**, *8*, 676.
(42) Knebel, A.; Wulfert-Holzmann, P.; Friebe, S.; Pavel, J.; Strauß, I.; Mundstock, A.; Steinbach, F.; Caro, J. Hierarchical Nanostructures of Metal-Organic Frameworks Applied in Gas Separating ZIF-8-on-ZIF-67 Membranes. *Chem.—Eur. J.* **2018**, *24*, 5728−5733.
(43) Shekhah, O.; Hirai, K.; Wang, H.; Uehara, H.; Kondo, M.; Diring, S.; Zacher, D.; Fischer, R. A.; Sakata, O.; Kitagawa, S.; Furukawa, S.; Wöll, C. MOF-on-MOF heteroepitaxy: perfectly oriented $Zn_2(ndc)_2(dabco)_n$ grown on $Cu_2(ndc)_2(dabco)_n$ thin films. *Dalton Trans.* **2011**, *40*, 4954−4958.
(44) Yao, M.-S.; Xiu, J.-W.; Huang, Q.-Q.; Li, W.-H.; Wu, W.-W.; Wu, A.-Q.; Cao, L.-A.; Deng, W.-H.; Wang, G.-E.; Xu, G. Van der Waals Heterostructured MOF-on-MOF Thin Films: Cascading Functionality to Realize Advanced Chemiresistive Sensing. *Angew. Chem.* **2019**, *131*, 15057−15061.
(45) Wang, Z.; Liu, J.; Lukose, B.; Gu, Z.; Weidler, P. G.; Gliemann, H.; Heine, T.; Wöll, C. Nanoporous designer solids with huge lattice constant gradients: multiheteroepitaxy of metal-organic frameworks. *Nano Lett.* **2014**, *14*, 1526−1529.
(46) Oldenburg, M.; Turshatov, A.; Busko, D.; Wollgarten, S.; Adams, M.; Baroni, N.; Welle, A.; Redel, E.; Wöll, C.; Richards, B. S.; Howard, I. A. Photon Upconversion at Crystalline Organic-Organic Heterojunctions. *Adv. Mater.* **2016**, *28*, 8477−8482.
(47) Ikigaki, K.; Okada, K.; Tokudome, Y.; Toyao, T.; Falcaro, P.; Doonan, C. J.; Takahashi, M. MOF-on-MOF: Oriented Growth of Multiple Layered Thin Films of Metal-Organic Frameworks. *Angew. Chem.* **2019**, *131*, 6960−6964.
(48) Tu, M.; Wannapaiboon, S.; Khaletskaya, K.; Fischer, R. A. Engineering Zeolitic-Imidazolate Framework (ZIF) Thin Film Devices for Selective Detection of Volatile Organic Compounds. *Adv. Funct. Mater.* **2015**, *25*, 4470−4479.
(49) Keppler, N. C.; Hindricks, K. D. J.; Behrens, P. Large refractive index changes in ZIF-8 thin films of optical quality. *RSC Adv.* **2022**, *12*, 5807−5815.
(50) Vandezande, W.; Janssen, K. P. F.; Delport, F.; Ameloot, R.; De Vos, D. E.; Lammertyn, J.; Roeffaers, M. B. J. Parts per Million Detection of Alcohol Vapors via Metal Organic Framework Functionalized Surface Plasmon Resonance Sensors. *Anal. Chem.* **2017**, *89*, 4480−4487.
(51) Demessence, A.; Boissière, C.; Grosso, D.; Horcajada, P.; Serre, C.; Férey, G.; Soler-Illia, G. J. A. A.; Sanchez, C. Adsorption properties in high optical quality nanoZIF-8 thin films with tunable thickness. *J. Mater. Chem.* **2010**, *20*, 7676−7681.
(52) Morris, W.; Doonan, C. J.; Furukawa, H.; Banerjee, R.; Yaghi, O. M. Crystals as molecules: postsynthesis covalent functionalization of zeolitic imidazolate frameworks. *J. Am. Chem. Soc.* **2008**, *130*, 12626−12627.
(53) Wang, J.; Zang, W.; Xi, S.; Kosari, M.; Pennycook, S. J.; Zeng, H. C. Trimetal atoms confined in openly accessible nitrogen-doped carbon constructs for an efficient ORR. *J. Mater. Chem. A* **2020**, *8*, 17266−17275.
(54) Thommes, M.; Kaneko, K.; Neimark, A. V.; Olivier, J. P.; Rodriguez-Reinoso, F.; Rouquerol, J.; Sing, K. S. Physisorption of gases, with special reference to the evaluation of surface area and pore size distribution (IUPAC Technical Report). *Pure Appl. Chem.* **2015**, *87*, 1051−1069.
(55) Kaenphakdee, S.; Putthithanas, P.; Yodyingyong, S.; Leelawattanachai, J.; Triampo, W.; Sanpo, N.; Jitputti, J.; Triampo, D. Zinc Oxide Synthesis from Extreme Ratios of Zinc Acetate and Zinc Nitrate: Synergistic Morphology. *Materials* **2022**, *15*, 570.
(56) Strauss, I.; Mundstock, A.; Hinrichs, D.; Himstedt, R.; Knebel, A.; Reinhardt, C.; Dorfs, D.; Caro, J. The Interaction of Guest Molecules with Co-MOF-74: A Vis/NIR and Raman Approach. *Angew. Chem., Int. Ed.* **2018**, *57*, 7434−7439.
(57) Tao, J.; Wang, X.; Sun, T.; Cai, H.; Wang, Y.; Lin, T.; Fu, D.; Ting, L. L. Y.; Gu, Y.; Zhao, D. Hybrid Photonic Cavity with Metal-Organic Framework Coatings for the Ultra-Sensitive Detection of Volatile Organic Compounds with High Immunity to Humidity. *Sci. Rep.* **2017**, *7*, 41640.

https://doi.org/10.1021/acs.cgd.2c00664
Cryst. Growth Des. 2022, 22, 7008−7020